Journal of Engineering Research

Volume 7 | Issue 2 Article 44

2023

Enhancing the Behavior of R.C. Continuous-Defected Slabs Using Strain-Hardening Cementitious Composites (SHCC)

mahmoud A aziz,

Journal of Engineering Research (ERJ)
Vol. 7 – No. 2, 2023
©Tanta University, Faculty of Engineering
ISSN: 2356-9441 https://erjeng.journals.ekb.eg/ e ISSN: 2735-4873

Enhancing the Behavior of R.C. Continuous-Defected Slabs Using Strain-Hardening Cementitious Composites (SHCC)

Mahmoud A. Abdel-Aziz[1], Emad Etman[2], Mohammed Hussein[3], and Nesreen Kassem[4]

[1]Assistant Professor, Faculty of Engineering, Tanta University, Egypt. – email: Mahmoud.Abdelaziz@f-eng.tanta.edu.eg
[2]Professor, Structural Engineering Department, Faculty of Engineering, Tanta University, Egypt.
[3]Professor, Structural Engineering Department, Faculty of Engineering, Tanta University, Egypt.
[4]Professor, Structural Engineering Department, Faculty of Engineering, Tanta University, Egypt.

***Abstract*- Defected continuous slabs resulting from mistakes in the position of upper reinforcement over their intersection with beams can be repaired with many alternatives. Strain Hardening cementitious composite (SHCC) is among the modern alternatives appeared in the last years. This Paper highlights test results of nine double-span one-way reinforced concrete (R.C.) slabs tested under five- point where the control slab was manufactured without top reinforcement at the inner support. The main studied parameters were the position of SHCC layer relative to the concrete section, the thickness of SHCC layer, reinforcement ratio in SHCC layer, and development length of SHCC layer. The results showed that using SHCC layer with reinforcement ratios 0.38%, 0.5%, and 0.63% increases the cracking load in the positive region by 50%, 57.7%, and 69.5%, the cracking load in the negative region by 88.4%, 100%, and 111.5%, the ultimate load by 31.4% and 41.43%, and 58.6%, and the ductility by 16.8%, 86%, and 147%, respectively, compared to the control slab. It isn't prescribed to lessen the development length of the SHCC layer to 0.15 of the clear spans because the slab failed outside the strengthening layer. The flexural capacity of the test slabs is generally underestimated by the suggested flexural prediction model based on forces equilibrium. The analytical/experimental results' average value ranged from 0.8 to 0.9, providing a good margin of error.**

***Keywords*- Improving, Strengthening, Ductility, One-way, Line-loads, Solid Slabs.**

I- INTRODUCTION

Neglecting to place or inefficiency of upper reinforcement in continuous solid slabs due to construction mistakes are likely to occur. In these slabs, the loads were supported by the reinforcement of the sagging moments only. So, the deficit in slab continuity weaken the slabs' ability to withstand against loads and increase slabs deflection [1]. To restore the flexural strength of these slabs, careful consideration must be given to a suitable strengthening strategy.

To increase the strength of RC slabs with defects, many strengthening procedures have been devised. One of the typical reinforcing techniques for RC slabs is to add a fresh layer of concrete [2]. A fresh concrete layer next to an older concrete part, however, might result in durability issues like delamination or cracking along the contact surface between the two materials. This is attributable to the differing movements of the new overlay and the concrete substrate as a result of temperature changes, shrinkage, or both [3,4]. Therefore, employing appropriate shear connections between the two layers and/or performing excellent surface preparation is crucial [5]. Steel plates that are externally bonded (EB) are another way of reinforcement. In this method, the steel plates can be attached either by adhesive bonding or bolting. Previous studies have shown that EB steel plates are efficient in reducing cracks width and deformations at all load levels while also increasing flexural capacity [6,7]. External steel plates, however, are prone to corrosion damage, necessitating additional protection costs. In addition, stress concentration in the anchorage zone is created if mechanical anchorage is utilised rather than epoxy glue [8].

FRP materials provide a number of advantages, including high strength, low weight, and resistance to corrosion. There are several modern uses for these materials that make use of these benefits. The Externally Bonded (EB) approach was used because of how easy it is to install. Several research have reported on the flexural response of RC slabs with defects reinforced with EB-CFRP sheets [9–11]. According to their observations, the FRP-strengthened slabs outperformed their un-strengthened counterparts in terms of load-carrying capacity. However, the majority of the FRP-reinforced slabs collapsed due to the FRP debonding from the concrete slab. To prevent debonding failure, the Near Surface Mounted (NSM) approach has been used. In the NSM process, pre-cut grooves that are orientated along the concrete cover are filled with filler material and reinforcing bars or strips. Less hostile environments are exposed to the NSM approach. The NSM approach also has a better bond efficiency than the EB technique because it has a larger surface area in contact with the substrate concrete. As a result, debonding failures are more likely to occur with the EB method than with NSM FRP strips [12]. FRP materials do, however, still have significant limitations, such as high cost, concrete surface agent, limited fire resistance, which necessitates high fire prevention costs [13].

Engineered cementitious composites (ECC) are micromechanically engineered composite materials mixed with random short fibres that have a fibre volume fraction of less than 2-3% and exhibit different cracking behaviours as well as tensile strain hardening properties [14]. The strain hardening cementitious composite (SHCC) has various pros. Their maximum tensile strain is up to 5%, which is substantially higher than the maximum tensile strain of

DOI: 10.21608/ERJENG.2023.212986.1182

Journal of Engineering Research (ERJ)
Vol. 7 – No. 2, 2023
©Tanta University, Faculty of Engineering
ISSN: 2356-9441 https://erjeng.journals.ekb.eg/ e ISSN: 2735-4873

typical concrete [14]. In contrast to regular RC beams, many small cracks are anticipated to occur on the tensile side of RC members when SHCC are applied [15]. The sparsely spaced small cracks will effectively disperse stress throughout the FRP jacket and reduce crack-induced stress concentration. Due to these qualities, SHCC is an excellent repair material [16]. The ability to adjust crack width, high deformation, high damage tolerance, energy absorption, delamination resistance, shear load resistance, and high durability are just a few of the advantageous traits of SHCC that researchers have found to be useful in reinforcing or repairing structures. For instance, Lim and Li [17] discovered that SHCC were successful at trapping interface fractures, hence eradicating frequent failure modes in a SHCC/concrete strengthening system, such as early or surface spalling, and extending the system's service life. According to Suthiwarapirak et al. [18], SHCC has a substantially higher capacity for fatigue resistance than conventional repairing materials. SHCC can also reduce shrinkage crack width and are freeze-thaw resistant [19]. The usage of integrated steel reinforcement within SHCC members was advised by various researches [20,21].

According to Fischer and Li [22], components made of SHCC with steel reinforcement shown improved tension stiffening behaviour. This means that the structural performance of steel/SHCC composite components was improved as a result of steel reinforcement. The usefulness of steel reinforcement in enhancing the post-cracking stiffness and post-ultimate ductility of specimens exposed to direct stress was demonstrated by Kunieda et al. [23]. The effectiveness of SHCC-enhanced elements has been assessed in laboratory testing through a variety of investigations, which showed improved structural performance when SHCC material was used [24–26]. Review research on the mechanical characteristics of fiber-reinforced concrete was published by Abbas and Khan [27]. Chung et al. [28]investigated the impact of specimen shapes on the compressive strength of designed cementitious composites with various water-to-binder ratio values.

A number of research have sought to use SHCC as a repair material to enhance masonry walls, RC beams, or RC frames, but one of the most often employed applications of SHCC may be reinforcing building structures. For instance, Maalej et al. [29] found that the proposed SHCC strengthening techniques successfully increased the bearing capacity and ductility of the unreinforced masonry walls under a variety of low-velocity loads, averting brittle and catastrophic collapse. The efficiency of RC frames with masonry fill that have been fortified with SHCC is examined by Dehghani et al. in their study from [30]. Test findings show that an SHCC strengthening system may greatly increase the lateral strength and energy dissipation capabilities of an infilled frame, hence eliminating brittle failure modes of the infill wall. Kesner and Billington [31] introduced a precast panel infill solution for critical frame structures that uses SHCC materials rather than traditional concrete materials. Along with other structurally enhancing materials like FRP, SHCC may also be utilised as a composite reinforcement material to strengthen the structures. Maalej and Leong [32] performed experimental tests on the behaviour of FRP-strengthened RC beams with SHCC added as a ductile jacket cast on the beam bottom. Numerous, thin fractures appeared on the beam's tensile surface, which helped to evenly distribute stress throughout the FRP jacket and lessen crack-induced stress concentration. Dai et al. [33] evaluated the flexural performance of RC beams reinforced with textile reinforced SHCC (TRSHCC), and they found that the creation of numerous microscopic cracks in the SHCC improved the ductility of this strengthening system.

Khalil. Et al. [26] Creating a cut-out in an existing RC slab and repair it by a new technique based on near surface mounted has precast plates made of SHCC. The results showed that he use of the SHCC plates at the tension side only increased the load-carrying capacities of the slabs with cut-outs to reach about 95% of that attained by the control slab for slabs with cut-outs. However, this increase was accompanied by a significant decrease in the ductility. Sabry Fayed [1] conducted an experimental program to study the Flexural Strengthening of Defected RC Slabs Using SHCC. The results showed that using SHCC layer delayed the failure occurrence compared to the unstrengthened specimen, and the cracks were distributed in a bigger area. Also, the first crack of the strengthen slabs was higher than that of the reference slab. Using a reinforcement ratio of the SHCC layer by 1.25–1.88% increased the ultimate carrying load of the slabs by 18.18–27.27%, respectively.

Finally, and from the previous review, for some reasons due to mistakes conducted during the construction phase unintentionally, is possible for slabs to lose the advantages of continuity and slabs behave as if they were simple squiggles but not fully disconnected in moments. The slab system didn't collapse under vertical loads until plastic hinges formed at the sagging moment zones, but at service loads, large-width crack occurs follow the distribution of the ceiling beams. The optimum solution to restore these roofs is strengthening the hogging moments' zones. In the current research, an experimental investigation was carried out to study the structural behaviour of continuous R.C. slabs without upper reinforcement strengthened in hogging moment region using SHCC layer with different parameters.

II- RESEARCH SIGNIFICANCE

This paper reports test results of nine double-span one-way RC slabs tested under five-point loading where the control slab was manufactured without upper reinforcement at the inner support. The control slab is similar to a condition likely to occur in filed due to mistakes conducted during the construction phase unintentionally. The paper focuses on describing the behaviour of eight specimens strengthened at the hogging moment zone by SHCC layer as it is a one of modern and ductile alternatives. The position of the layer in relation to the concrete section, the thickness, the internal reinforcement ratio, and the length were studied parameters. The experimental results are checked against a suggested analytical procedure.

DOI: 10.21608/ERJENG.2023.212986.1182

Journal of Engineering Research (ERJ)
Vol. 7 – No. 2, 2023
©Tanta University, Faculty of Engineering
ISSN: 2356-9441 https://erjeng.journals.ekb.eg/ e ISSN: 2735-4873

III- EXPERIMENTAL PROGRAM

A. *Materials Properties*

The concrete mix composition is demonstrated in Table 1. The concrete of test slabs was normal strength concrete. Cement was mixed with dolomite, sand then, water was added. six cylinders with a diameter of 150 mm and a height of 300 mm and three cubes with a length of 150 mm were manufactured and tested by a compression testing machine to evaluate the concrete tensile and compressive strength. The average concrete compressive strength at the same time of slab testing was 30 MPa, and the average splitting tensile strength was 3.38 MPa.

The mix attributes of SHCC are shown in Table 1. The SHCC mixture was composed of regular Portland cement, fine silica sand with a grain size less than 0.42 mm, silica fume with an average diameter of 0.02 mm, polypropylene (PP) fibres, water, and superplasticizers. The SHCC binder was composed of fly ash and normal Portland cement 42.5R. Using a high range water reducer increased the flowability of the SHCC binder (HRWR). SHCC, a high strength PP fibre, was selected and accounted for 1% of the mixture. The PP fibres were 12 mm in length and 25 m in diameter. The PP fibres had maximum values for tensile strength, fibre elongation, and modulus elasticity of 2900 MPa, 2.42 percent, and 116 GPa, respectively. The water to binder ratios at SHCC were 0.2. The manufacturer has supplied a list of the exact fibre qualities in Table 2. During the mending phase, samples of the SHCC mix were produced in order to assess the tensile and compressive parameters. To prevent the size effect on the ultimate tensile strain of SHCC material, Li et al. [21]and Kunieda et al. [23]recommended doing the uniaxial tensile tests on big size specimens. The proposed size has a cross-sectional area of 50×200 mm and a length of 900 mm. Direct uniaxial tensile testing on three specimens were performed in line with [21,23]'s suggestions. Figures 1a, 1b, 1c, and 1d show, respectively, the observed tensile stress-strain curves for the SHCC specimens under test and the details of the axial tension test. According to Figure 1d, the average first-cracking strength, ultimate tensile strength, and total tensile strain of the utilised SHCC were 3.01 MPa, 6.45 MPa, and 6.4%, respectively. The compressive tests also made use of three cylinders. The specimen is 50 mm in diameter and 100 mm in height. The average compressive strength of the tested specimens was 62.74 MPa. Rebar D10 and D8 mm was tested under direct tension by Universal Testing Machine, and its attributes were provided in Table 3.

One of the key elements influencing the restoration procedure is the connection between the healing material and the substrate concrete. Following ASTM C882-99 guidelines, three cylindrical specimens underwent slant shear testing. The first half of the cylinder was cast using the same concrete mix that was utilized to create the tested specimens. Following a 28-day period, a mattock was used to roughen the contact surface (roughening depth was 5 mm). Within 15 minutes, the epoxy glue had been applied to the concrete basis, which had been prepared beforehand. Use of Kemapoxy 103, a structural resin epoxy, was made. The epoxy's initial and final setting durations are 15 and 60 minutes, respectively, according to the manufacturer's guidelines, and its density is 1.1±0.02 kg/L. After 28 days, a compression test was performed on the samples. Average slant shear strength was 16.85 MPa, and splitting failure occurred without sliding in the loading direction.

Table 1. Mix proportions of the N.S.C and SHCC materials (kg/m3) for cubic meter.

Mix	Water-to-binder ratio	Water	Super plasticizers	Expansion agent	Fibres (volumetric	Silica fume	Dolomite (kg/m^3)	Sand	Cement
NSC	0.66	175	-	-	-	-	1295	637	350
SHCC	0.2	292	14.6	20	14.6 (1%)	223	-	149	1243

Table 2. Properties of PP fibres.

Fiber	Diameter *df* (µm)	Length *Lf* (mm)	Aspect ratio *Lf/df*	Experimental strength	Nominal Young's	Elongation at breakage	Specific gravity	Oil coating (%)	Melting point (°C)
PP Fiber	25	12	720	2900	116	2.42	0.97	/	150

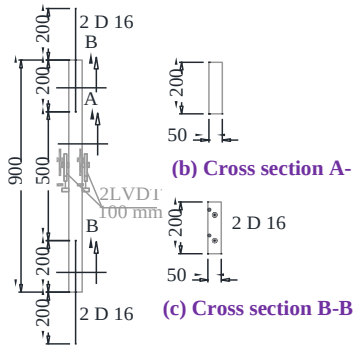

(b) Cross section A-

(c) Cross section B-B

(a) Reinforcement and dimensions of axial tension specimens

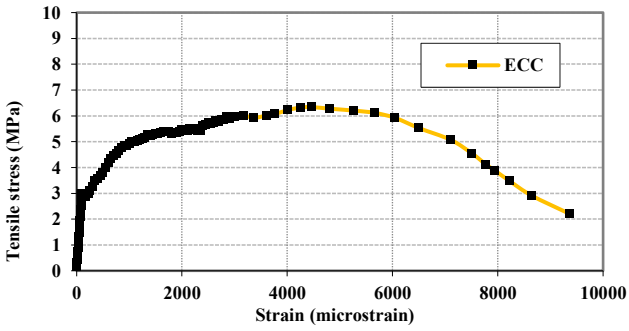

(d) Axial tension test's stress–strain curves

Fig. 1: Specimen's detailing and axial tension test's stress–strain curves.

DOI: 10.21608/ERJENG.2023.212986.1182

Journal of Engineering Research (ERJ)
Vol. 7 – No. 2, 2023
©Tanta University, Faculty of Engineering
ISSN: 2356-9441 https://erjeng.journals.ekb.eg/ e ISSN: 2735-4873

Table 3. Steel reinforcement's characteristics

Diameter, mm	Yield strength, MPa	Ultimate strength, MPa	Modulus of elasticity, GPa
8	253	355	205
10	374	564	205

B. Test slabs

The experimental program consists of nine R.C. slab representing a strip of 500 mm width, a thickness of 80 mm, and a total length of 2300 mm. The strip was tested under five-point loading, representing a continuous strip of a double-span one-way solid slab. The single span length is 1100 mm. All slabs are designed according to the ECP-203-2018 Code, but the presence of negative moment reinforcement has been ignored. All RC slabs were reinforced by main bottom high strength steel 4D10 mm in the longitudinal direction, which was chosen close to the maximum amount of reinforcement. The longitudinal bars were covered and fixed by distributed bars D10@220 mm in the traverse direction. As mentioned later, all slabs were designed without top reinforcement at the negative moment region over the inner support. The typical concrete dimensions and general reinforcement details for all RC slabs were illustrated in Fig. 2. The control slab (S_1) was left without strengthening. The other eight slabs were strengthened with SHCC layer at the middle-support. Details of test slabs were listed in Table 4.

Four main parameters were targeted in this study. The SHCC layer in this paper was overlayed after removing a similar layer from all slabs except in S_2, so that the total thickness of these slab does not increase after strengthening operation. The SHCC layer was poured to sit outside the section in S_2, while in other slabs the SHCC layer formed the upper part of the section without an increase in the total thickness. Figure 3a, 3b illustrate details of slab S_2 and other slabs, respectively. The second parameter was the SHCC layer thickness (t_{SHCC}). Slabs S_3, S_4, and S_5 had the same dimensions and reinforcement details as the control slab, while a different thickness of SHCC layers of 20 mm, 30 mm, and 40 mm, respectively was chosen. The SHCC layer thickness-to-the original slab thickness ratios were 25%, 37.5%, and 50% for slabs S_3, S_4, and S_5, respectively. The third parameter was the steel reinforcement ratio impeded in the SHCC layer. The slabs S_4, S_6, and S_7 have the same thickness of 30mm of the SHCC layer, but these layers were reinforced (A_s) by 3D8 mm, 4D8 mm, and 5D8 mm, respectively. The reinforcement ratios (ρ%) relative to the original slab thickness were 0.38%, 0.5%, and 0.63% for slabs S_4, S_6, and S_7, respectively. The last parameter was the development length of SHCC layer. Slabs S_4, S_8, and S_9 are typical, but SHCC layer were overlaid by development length (L_d) $0.25L_n$, $0.2L_n$, and $0.15L_n$ (where L_n is the span=1100 mm), respectively. The largest development length is taken according to ECP-203/2018 [34]. The study of smaller development lengths aims to reduce the cost of implementation while monitoring the change in the structural behaviour of the strengthed slabs.

Table 4. Test slabs

Slab	Original slab thickness (mm)	Total thickness after strengthening (mm)	SHCC thickness (t_{SHCC} mm)	SHCC reinforcement (As, ρ %)	Development length (L_d m)
S_1	80	Not strengthed	-	-	-
S_2	80	110	30	3D8; ρ=0.38%	0.25 L
S_3	80	80	20	3D8; ρ=0.38%	0.25 L
S_4	80	80	30	3D8; ρ=0.38%	0.25 L
S_5	80	80	40	3D8; ρ=0.38%	0.25 L
S_6	80	80	30	4D8; ρ=0.5%	0.25 L
S_7	80	80	30	5D8; ρ=0.63%	0.25 L
S_8	80	80	30	3D8; ρ=0.38%	0.20 L
S_9	80	80	30	3D8; ρ=0.38%	0.15 L

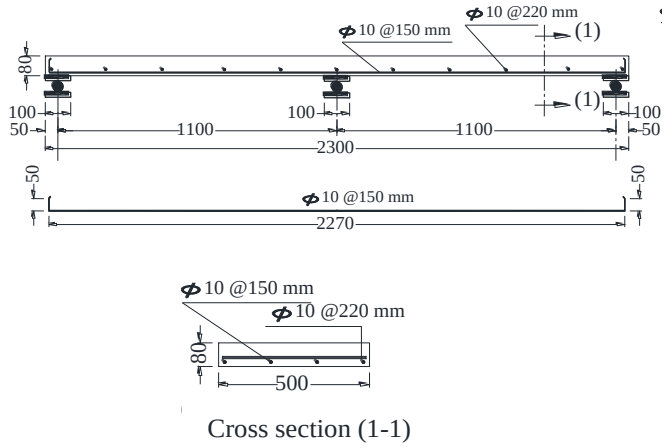

Fig. 2: Concrete dimensions and reinforcement detailing of Control slab S1, dim. in mm

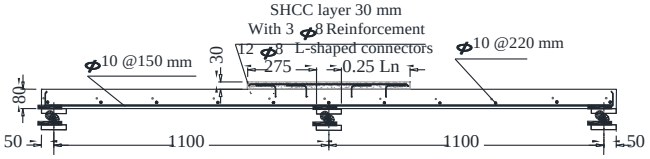

(a) Slab S_2

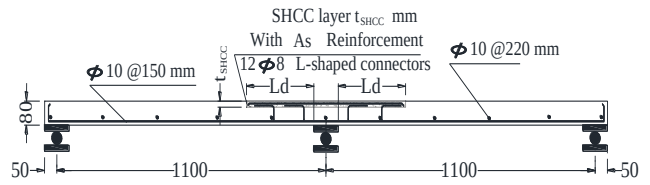

(b) Slab S_3 to S_9

Fig. 3: Concrete dimensions and reinforcement detailing of all slabs, dimensions in mm.

DOI: 10.21608/ERJENG.2023.212986.1182

Journal of Engineering Research (ERJ)
Vol. 7 – No. 2, 2023
©Tanta University, Faculty of Engineering
ISSN: 2356-9441 https://erjeng.journals.ekb.eg/ e ISSN: 2735-4873

Figure 4 shows Fabrication and preparation of test slabs. Counter panels were used to make the Formwork, as shown in the figure 4. The reinforcing cage was constructed in accordance with the plans, and after the surface had been thoroughly cleaned and polished, the strain gauge was bonded to the reinforcing steel using a special paste. The region was then sealed off with silicone to safeguard the strain gauge. then the reinforcing mesh was installed inside the formwork and the concrete was casted, figure 4a. Using ready-mixed concrete patch, all of the slabs were cast at once. Figure 3b show the test slabs after finishing the surface and roughing the strengthed area. Casting the SHCC layer begun 7 days after moulding the slabs. Concrete was drilled in specific locations according to slab details, with a diameter of 12 mm and a depth of 40 mm to install shear dowels, figure 4b. The hole was thoroughly cleaned of dust, by using a blower. An epoxy material was used to install the dowels according to the details, figure 4c. Also, the top surface of all slabs was roughened and clean well before dyeing an epoxy material to stick the SHCC layer to the original slabs well, figure 4d. Then, the SHCC layer was casted, figure 4e. All slabs were tested 28 days after the placing of the SHCC layer, and figure 4f shows Final slab shape.

(a) Finishing the surface and roughing the strengthed area

(b) Using the drill to make a concrete hole to install the dowels then cleaning the hole from dust by blower

(c) Install the dowels by epoxy

(d) Cleaning the area from dust by blower and paint the surface with epoxy.

(e) Installing the steel and casting the SHCC layer and finishing the surface

(f) Final slab shape

Fig. 4: Fabrication and preparation of test slabs

C. Details of the Test Setup and Instrumentation

The test program was implemented at the Reinforced Concrete Laboratory of the Faculty of Engineering, Tanta University. The instrumentations were placed at appropriate points of test slabs to get complete information about the slab behavior. Before casting concrete and SHCC layer, electrical resistance strain gauges were mounted on the longitudinal reinforcement at mid-span also on the reinforcement embedded in the SHCC layer to acquire steel strains, see figure 4b. The installation steps were preparing and cleaning the bar surface, fixing it by proper glue, and applying a thin coat of silicon for waterproofing. The overall test setup is shown in figure 5. Quick gypsum layers were installed before laying all loading plates to adjust the horizontality of the test slabs and to ensure uniform stresses at all points along with every loading plate. The two end supports of the test slab settled roller and the intermediate support subsided hinge. The dimensions of the plates employed for loading were 500 × 100 × 30 mm. The diameter and length of the utilized bar rod were 38 mm and 500 mm, respectively. The reaction of

DOI: 10.21608/ERJENG.2023.212986.1182

Journal of Engineering Research (ERJ)
Vol. 7 – No. 2, 2023
©Tanta University, Faculty of Engineering
ISSN: 2356-9441 https://erjeng.journals.ekb.eg/ e ISSN: 2735-4873

the middle support was obtained by a load cell installed under the support plate.

The deformation was measured by five Linear Variable Differential Transformers (LVDTs) fixed at mid-span points and the supports. The mid-span deflection is the result of subtracting the average reading of LVDTs at the adjacent supports from the reading of LVDT at the mid-span. The concrete strain gage of, 100mm length, was fixed at top of the mid-span section to obtain concrete strains at every loading level. A 250 kN hydraulic jack was utilized to apply the external load and the load value was obtained by a load cell attached to the hydraulic jack. This load was divided into equal two loads in order to operate every load at the mid of the two spans. The applied load at the column was applied incrementally and from time to time the crack propagations were marked up to failure, then the value of the load level was adorned at the end of each crack. Also, a crack measuring microscope was used to determine the crack width at planned load levels. All instrumentations were connected to a data acquisition system (D.A.S) then examined well. During the test, microelectronic signals were transmitted from instrumentation to the D.A.S then stored in a connected computer in an excel sheet.

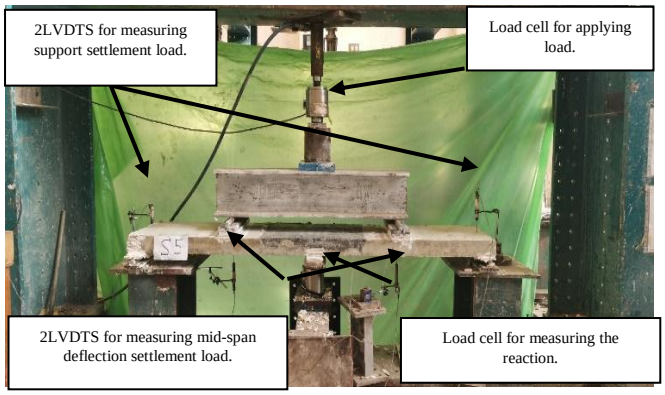

Fig. 5: Test setup

IV- EXPERIMENTAL RESULT AND DISCUSSION

All experimental results are listed in table 5. This section discusses the crack patterns and mode of failure, cracking loads, initial stiffness, and ultimate load capacity.

A. Crack Pattern and Mode of Failure

For the control slab S_1, the first crack appeared above the intermediate support owing to hogging moment at 26 kN (37% from the ultimate load P_{u1}) and rabidly another crack appeared at the maximum sagging moment zone under the applied load. There is no doubt that, the rapid appearance of the crack in the of the sagging positive moment is attributable to redistribution of hogging negative moments after cracking of the unreinforced section. Via increasing the applied load, the width and the depth of the first crack at negative moment increased without any increasing in cracks numbers until failure. on the other hand, the cracks number, width and depths at the positive moment zone increased until the cracks number reached three cracks at 58 kN (82%P_{u1}) then, the number remained constant until failure. The crack width in the negative and positive moments zones at a load of 45 KN (65%P_{u1}) was 0.4 and 0.2 mm, respectively, while at a load of 58 kN (82%P_{u1}), the crack width in the negative moments, and the width of the main crack in the positive moments was reached 0.6 and 0.3 mm, respectively and when the slab was close to collapse, the cracks width reached 1.2 mm and 0.5 mm, respectively.

At failure (70kN) it was noticed at the negative moments zone that, only a single crack developed from cracking until failure, and it is located in the middle of the intermediate support. noticing the three positive moment cracks, find that the middle crack appeared in the intermediate of the loading plate, and the other two, one on the right of the loading plate and the other on the left of it with a distribution distance of about 270 mm, a quarter of the clear span (0.25 L_n).

Table 5. Test results

Slab	Δ_{cr} (mm)	Δ_y (mm)	Δ_u (mm)	P_{cr+ve} (kN)	P_{cr-ve} (kN)	P_u (kN)	Initial stiffness (kN/mm)	D.F
S_1	1.77	5.02	7.79	26	26	70	14.7	1.55
	Mode of failure (Tension failure)							
S_2	2.013	4.03	5.55	42	59	100	20.9	1.38
	Mode of failure (Debonding of SHCC and Shear failure in the slab)							
S_3	2.29	4.1	6.76	38	47	91	16.6	1.65
	Mode of failure (Tension failure)							
S_4	2.32	4.13	7.46	39	49	92	16.8	1.81
	Mode of failure (Tension failure)							
S_5	2.31	4.16	7.91	39	49	93	16.8	1.90
	Mode of failure (Tension failure)							
S_6	2.25	4.25	12.7	41	52	99	18.2	2.98
	Mode of failure (Tension failure)							
S_7	2.13	4.41	16.9	44	55	111	20.7	3.83
	Mode of failure (Tension failure)							
S_8	2.32	4.1	7.52	39	48	93	16.8	1.83
	Mode of failure (Tension failure)							
S_9	2.26	4.27	4.27	37	45	62	16.4	1.00
	Mode of failure (Debonding of SHCC and Shear failure in the slab)							

DOI: 10.21608/ERJENG.2023.212986.1182

Journal of Engineering Research (ERJ)
Vol. 7 – No. 2, 2023
©Tanta University, Faculty of Engineering
ISSN: 2356-9441 https://erjeng.journals.ekb.eg/ e ISSN: 2735-4873

Through increasing the load up to failure, yield in positive steel arisen, no increase in the load noticed, and the slab showed a ductile behavior until the concrete failed at the compression zone. Then, the load was released. The failure was classified as tensile failure. Figure 6a illustrates the crack patterns of slab S_1 after failure.

When comparing the crack propagation of S_2 and S_4, where the SHCC layer was poured to sit outside the section in S_2, while in S_4 the SHCC layer was overlayed after removing a similar layer from the slab. Thus, after strengthening operation, the total thickness of slabs S_2 and S_4 were 120mm and 80 mm, respectively. For slabs S_2 and S_4 the first crack appeared at the positive moment at 40 and 37 kN, respectively (40% P_{u2} and 40.6%P_{u4}). Under loading, the first crack appeared at the negative moment zone at the intermediate support at 59 and 49 kN, respectively (59%P_{u2} and 53.2%P_{u4}).

(a) Crack pattern of specimen S1

(b) Crack pattern of specimen S2

(c) Crack pattern of specimen S3

(d) Crack pattern of specimen S4

(e) Crack pattern of specimen S5

(f) Crack pattern of specimen S6

(g) Crack pattern of specimen S7

(ا) Crack pattern of specimen S8

(j) Crack pattern of specimen S9

Fig. 6: Crack pattern of test slab

By increasing the applied load, the initial crack at the negative moment's breadth, depth grew, and the number of cracks increased. In both slabs S_2 and S_4, at a load of 81kN and 74 kN (81% P_{u2} or P_{u4}), the number of cracks at the negative moments zone and the positive moment's zone were 3 and 4 cracks. The distribution distance of the negative and positive moment cracks was about 160 mm and 290mm, respectively in S_2, 170mm and 300mm in S_4. The same number of cracks remained in the slabs until failure. For S4 at a load of 80 kN (87%P_{u4}), the crack width in the negative moments zone and the width of the main crack in the positive

DOI: 10.21608/ERJENG.2023.212986.1182

Journal of Engineering Research (ERJ)
Vol. 7 – No. 2, 2023
©Tanta University, Faculty of Engineering
ISSN: 2356-9441 https://erjeng.journals.ekb.eg/ e ISSN: 2735-4873

moment's zones were, respectively, 0.1 and less than 0.08 mm for S_4. For S_2 at the same load level at 87 kN ((87%P_{u2}), the crack width in the negative and positive moments zones is still behind 0.06 mm. At a load of 88 KN (96%P_{u4}), the crack width in the negative moments zone and the width of the main crack in the positive moments were, respectively, 0.4 and 1.8 mm for S_4.

When the slab was on the verge of collapsing, yield in the steel developed, no load increase was apparent, and the slab displayed ductile behaviour up until the concrete collapsed in the compression zone. For slab S2, the load reached 99 kN without a significant increase in the number, width, and depths of cracks. Up until a crack started to emerge between the SHCC layer and the slab's top surface at the negative moment zone. The slab with less thickness sustains the load after the strengthening layer splits then the slab falls abruptly due to shearing. Figures 6b and 6d illustrate the crack patterns of slab S_2, and S_4 respectively after failure.

For slabs S_3, S_4, S_5 which was strengthen by 20 mm, 30 mm and 40 mm of SHCC layer respectively, the first crack appeared at the positive moment under the applied load at 38 ,39 and 39 kN, respectively (41.7%P_{u3}, 42.4%P_{u4} and 41.9%P_{u5}). Under loading, the first crack appeared at the negative moment zone at the intermediate support at 47, 49, and 49 kN, respectively (51.6%P_{u3}, 53.2%P_{u4} and 52.7%P_{u5}). By way of increasing the applied load, the number, the width, and the depth of cracks at negative and positive moment zones increased. The total number of cracks up to failure was 3, 4 and 4 at the negative moment and 5 at positive moment zones for slabs S_3, S_4, S_5 respectively. The distribution distance of cracks at the positive moment was approximately 300 mm (0.27 L_n) for all slabs, while the negative moment cracks were distributed over a distance of about 150 mm (0.136 L_n) for all slabs.

The crack width for negative moment zone at a load of 80 kN (87.9%P_{u3}, 87%P_{u4} and 86%P_{u5}) was approximately 0.12 mm, 0.1 mm and 0.08 mm, respectively, but the crack width at positive moment zone at the same load was approximately 0.1 mm, 0.08 mm and 0.07mm, respectively. By increasing the load to 96% P_u, the crack width for negative moment zone was approximately 0.45 mm, 0.4 mm and 0.35 mm, respectively, but the crack width at positive moment zone at the same load was approximately 2.0 mm, 1.8 mm and 1.5 mm, respectively. Through increasing the load up to failure, yield in positive and negative steel arisen, negligible increase in the load noticed, and the slab showed a high ductile behavior until the concrete failed at the compression zones. Then, the load was released. The failure was classified as tensile failure for all slabs. Figures 6c, 6d and 6e illustrate the crack patterns of slab S_3, S_4, and S_5 respectively after failure.

The first crack developed at the positive moment under the applied load for slabs S_4, S_6, and S_7 that its SHCC layer were reinforced by 3D8, 4D8, and 5D8, respectively at 39, 41 and 44 kN (42.4%P_{u4}, 41%P_{u6}, and 39.6%P_{u7}). The first crack developed at the intermediate support's negative moment zone at loads of 49, 52, and 55 kN (53.2%P_{u4}, 52%P_{u6}, and 49.5%P_{u7}), respectively. The number, width, and depth of cracks at the negative and positive moment zones increased when the applied load was increased. For slabs S_3, S_4, and S_5, the total number of cracks up until failure was 4 in the negative moment zones and 5, respectively, at the positive moment zones. For the slabs, the positive moment crack distribution distance was around 300 mm (0.27 L_n), whereas the negative moment crack distribution distance was roughly 150 mm (0.136 L_n). Positive moment zone crack widths at the load of 80 kN were around 0.08 mm, 0.07 mm, and 0.07 mm, respectively, whereas the negative moment zone crack widths were roughly 0.1 mm, 0.09 mm, and 0.08 mm, respectively. The fracture width in the negative moment zone decreased to roughly 0.4 mm when the load was increased to 96% P_u, however the crack width in the positive moment zone increased to approximately 1.8 mm. As the load was increased until failure, yield in the positive and negative steel developed, the load barely increased, and the slab displayed remarkable ductility until the concrete collapsed at the compression zones. For all slabs, the mode of failure was identified as a tension failure. Figures 6d, 6f, and 6g show the crack patterns of slabs S_4, S_6, and S_7 following failure, respectively.

For slabs S_4, S_8, and S_9 having SHCC layers with development lengths of 0.25L_n, 0.2L_n, and 0.15L_n, at corresponding loads of 39, 39, and 37 kN (42.4 %P_{u4}, 41.9%P_{u8}, and 59.7%P_{u9}), the first crack appeared at the positive moment under the applied load. At loads of 49, 48, and 45 kN (53.2%P_{u4}, 51.6%P_{u8}, and 72.6%P_{u9}), the intermediate support's negative moment zone saw the onset of the first crack, correspondingly. As the applied load was raised, the quantity, breadth, and depth of fractures at the negative and positive moment zones grew. Up to failure, there were a total of 4 cracks in the negative moment zones and 5, correspondingly, in the positive moment zones for slabs S_4 and S_8, but S_9 showed only a total of 4 cracks in the negative moment zones and 2 correspondingly, in the positive moment zones. Slab S_8 showed the same behavior as S_4 up to failure. In case of S_9, just the load reached 59 kN a crack started at the end of the development length to emerge between the SHCC layer and the slabs at the negative moment zone. Because the slab with less thickness (50 mm) sustains the load after the strengthening layer splits, the slab falls abruptly due to shearing. Figures 6i and 6j illustrate the crack patterns of slab S_8, and S_9 respectively after failure.

B. Cracking load Comparison

Figure 7a illustrates the impact of the studied parameters (position of SHCC layer in relation to concrete section and thickness of SHCC layer) on the cracking loads of the reinforced slabs. The ratio between the first cracking load of the targeted specimen (P_{cri}) and the first cracking load of the reference specimen (P_{cr1}) was indicated on the vertical axis. The P_{cr1} is the initial cracking load of the reference specimen slab S_1 that has not been reinforced in the negative moment zone at the internal support. For each slab, two columns were produced, the first of which displayed the cracking moment ratios in the positive moment zone and the other of which displayed them in the negative moment zone above the inner support.

DOI: 10.21608/ERJENG.2023.212986.1182

Journal of Engineering Research (ERJ)
Vol. 7 – No. 2, 2023
©Tanta University, Faculty of Engineering
ISSN: 2356-9441 https://erjeng.journals.ekb.eg/ e ISSN: 2735-4873

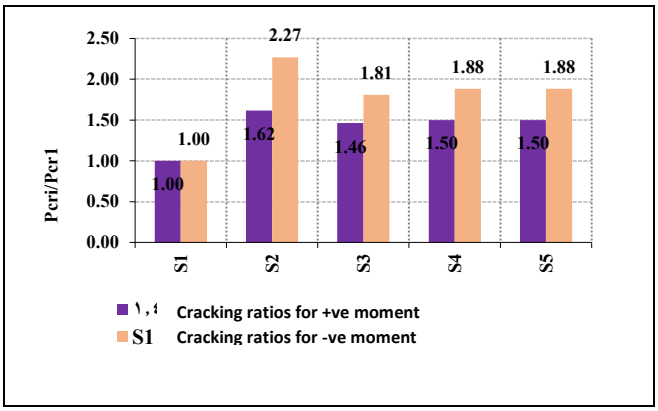

(a)

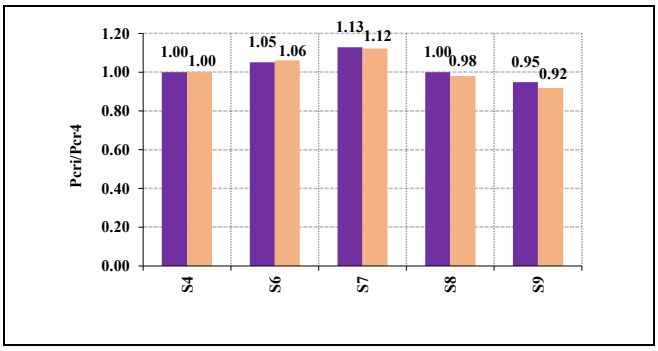

(b)

Fig. 7: Effect of the studied parameters on the crack load of the test slabs

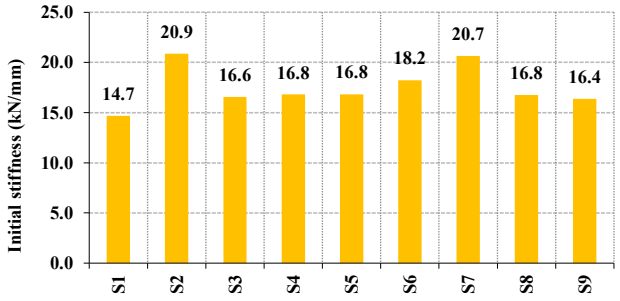

Fig. 8: Initial stiffness (kN/mm) of the test slabs

According to the graph, adding a layer of SHCC with a thickness of 30 mm (37.5% of the slab thickness) to slabs with an 80 mm thickness delays the first cracking load by an additional 62% and 127% in both sagging and hogging moment respectively. The initial cracking load was also postponed by flexural strengthening, which involved replacing a portion of the original concrete section with varying depths of SHCC layer and continual internal reinforcements. The increase ratio was 46% and 81% for slab strengthed by SHCC layer thickness-to-the original slab thickness ratios 25% in both sagging and hogging moment respectively. The initial cracking loads of the slab in both sagging and hogging moment respectively were not appreciably delayed by using a layer thickness more than 25% of the slab thickness.

The effect of the investigated parameters on the cracking loads of the reinforced slabs is shown in figure 7b, including the reinforcement ratio in the SHCC layer and the development length of the SHCC layers. The vertical axis displayed the ratio between the first cracking load of the targeted specimen (P_{cri}) and the initial cracking load of the reference specimen (P_{cr4}). P_{cr4} is the first cracking load of slab S_4, the reference specimen, which was the internal support's negative moment zone has been strengthened by 30 mm SHCC layer with reinforced ratio 0.38%. Also, two columns were created for each slab, the first of which showed the cracking moment ratios in the positive moment zone and the other of which showed them in the negative moment zone. The graph shows that the initial cracking load is delayed by an extra 5-6% and 12-13% by increasing the reinforcement ratios from 0.38% to 0.5%, and 0.63% respectively (reinforcement ratio increased by 31.6% and 65.8% for S_6, and S_7, respectively) in both sagging moment and hogging moment. By comparing S_4, S_8 and S_9, the cracking moment reduces by 5% and 8% in the sagging moment and hogging moment, respectively, when the developing length is reduced from $0.25L_n$ to 0.15. Except when the development length is shortened to $0.15L_n$, the SHCC layer's development length has no discernible impact on the value of the cracking in both sagging and hogging moments.

C. Initial stiffness

The elastic modulus of the concrete and the cross section-section thickness has the most effects on the slabs's initial stiffness. The initial stiffness, one of the vital comparison indicators, is calculated by dividing the first flexural cracking load of the beam by the first flexural cracking deflection value. Table 5 also provides a summary of the first cracking load values, mid-span deflection at cracking loads, and computed starting stiffness. A graph of the tested beams' initial stiffness is shown in Figure 8.

According to the computations, S_1 and S2 have starting stiffnesses of 14.7, and 20.9 kN/mm, respectively. The graph shows that the initial stiffness is increased by 42.1% when a layer of SHCC with a thickness of 30 mm (37.5% of the slab thickness) is added above the slabs with an 80 mm thickness for $0.25L_n$. The thickness of the SHCC layer that was replaced by a portion of the original concrete section without increasing the thickness of the slab and the reinforcement ratio in the SHCC layer increased by 14.2% compared to the initial stiffness of the control slab S_1. The graph shows also that the initial stiffness increased by an extra 8.3% and 23.2% by increasing the reinforcement ratios from 0.38% to 0.5%, and 0.63% respectively (reinforcement ratio increased by 31.6% and 65.8% for S_6, and S_7, respectively). When a strengthening layer used with a development length of 0.15 L_n or $0.20L_n$ instead of a layer with a development length of 0.25 L_n, the initial stiffness was reduced by 2.3% and 0%, respectively.

D. Ultimate Load Comparison

The effect of the investigated parameters (location of the SHCC layer relative to the concrete section and thickness of

DOI: 10.21608/ERJENG.2023.212986.1182

Journal of Engineering Research (ERJ)
Vol. 7 – No. 2, 2023
©Tanta University, Faculty of Engineering
ISSN: 2356-9441 https://erjeng.journals.ekb.eg/ e ISSN: 2735-4873

the SHCC layer) on the ultimate loads of the strengthed slabs is shown in Figure 9a. The vertical axis displayed the ratio between the ultimate load of the targeted specimen (P_{ui}) and the ultimate load of the reference specimen (P_{u1}). P_{u1} is the ultimate load of slab S_1. The graph shows that the ultimate load is increased by 47%, when a layer of SHCC with a thickness of 30 mm (37.5% of the slab thickness) is added above the slabs with an 80 mm thickness. The failure mode was controlled by separation in the strengthening layer, and it was possible to increase the load more than this value if this type of failure was avoided. It is recommended to make another program to study this point accurately. Flexural strengthening, which comprised replacing a part of the original concrete section with variable depths of SHCC layer and continuous internal reinforcements, also helped to increase the ultimate load. The increase ratio for the slab reinforced by the SHCC layer thickness to the original slab thickness ratio of 25% was 30%. By adopting a layer thickness greater than 25%, the ultimate load of the slab was not noticeably increased.

Figure 9b illustrates how the analyzed parameters (including the SHCC layer's development length and reinforcement ratio) affect the ultimate loads of strengthed slabs. The ratio between the ultimate load of the targeted specimen (P_{ui}) and the ultimate load of the reference specimen was shown on the vertical axis (P_{u4}). P_{u4} is the ultimate load of slab S_4, the reference specimen, which had a 30 mm SHCC layer with a reinforced ratio of 0.38% added to enhance the internal support's negative moment zone. The graph demonstrates that increasing the reinforcement ratios from 0.38% to 0.5% and 0.63%, respectively, increase the ultimate load by an additional 8% and 21% (reinforcement ratio increased by 31.6% and 65.8% for S6, and S7, respectively).

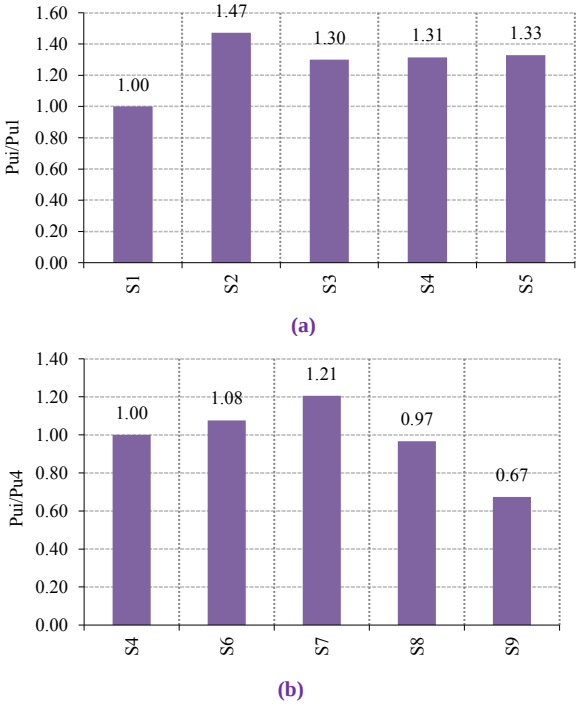

Fig. 9: Effect of the studied parameters on the ultimate load capacity of the test slabs

By comparing S_4, S_8, and S_9, it can be shown that when the developing length is decreased from $0.25L_n$ to 0.15, the ultimate moment decreases to 67%. The SHCC layer's development length has a negligible effect on the value of the ultimate load when it was decreased to $0.2L_n$.

E. Load-Deflection Response

The relation between the total applied load and the failed mid-span deflection for all slabs is depicted in Figure 10. The load deflection curves were drawn from the test start until the load began to decrease.

The stiffness of all specimens may be determined from the slope of the load-deflection curve. From figure 10a, the stiffness of the slab S_2 after cracking is the highest because the total slab thickness is increased after strengthening the specimen to 110 mm but in S_4 the slab still 80 mm thickness. Also, up to failure the stiffness of slab S_4 is higher than S_1 due to strengthening the negative moment with a material that contributed to resist the load on the negative moment region and having higher modulus of elasticity than concrete. The load 26 kN caused the slab S_1 to crack above the middle support that has no reinforcing and in the zones of positive moment, which led to excessive deflection, and the point associated to the cracking moment was clearly visible in the slab's curve. On the contrary, all slab strengthed on the negative moment zone retained their stiffness after cracking.

Comparing the deflection of the three specimens S_1, S_2, and S_4 (for example 5.59, 3.018, and 3.52 mm at the same loading level 60kN), it can be seen that the deflection of the specimens S_2 and S_4 is decreased by 46% and 37%, respectively, in comparison to the control specimen S_1. The curves show that up to 98% of the collapse load, the slabs S_1 and S_2 stiffness was maintained. The stiffness of the slab S_2 began to gradually decrease at load values of 92% of the ultimate load. finally, the failure of Slab S_2 was brittle due to debonding of SHCC layer but in case of S_1 and S_4 the post beak behavior was ductile and show extra deformations.

From figure 10b, the slabs S_3 and S_5 showed the same load-deflection behavior as slab S_4. As the thickness of the compensatory repair layer for the cross-section increases, the curves almost coincide with a slight improvement in the value of the loads and deflection.

From figure 10c, the stiffness of the strengthed slabs slightly increased by increasing the internal reinforcement ratio. Nearly 90% of the collapse load is where the benefit of increased internal reinforcement can be seen. More internal reinforcement can control cracks, boost the slab's capacity, and subsequently lessen deflection at the same load level. Additionally, by adding more internal reinforcement to the SHCC layer, the slab's post beak behavior is enhanced. This is evident from the slope of the curves after the maximum load.

From figure 10d, the behavior of slabs S_8 and S_4 behave identically, hence employing the $0.20L_n$ development length has the same result as the $0.25L_n$ advised by certain codes. This might result in cost savings because fewer materials are needed. But when the development length was shortened to $0.15L_n$, the difference in behavior became apparent. The slab

DOI: 10.21608/ERJENG.2023.212986.1182

Journal of Engineering Research (ERJ)
Vol. 7 – No. 2, 2023
©Tanta University, Faculty of Engineering
ISSN: 2356-9441 https://erjeng.journals.ekb.eg/ e ISSN: 2735-4873

to act with a thin thickness without an SHCC layer (50 mm only) and collapse at a load level lower than the S_1 slab, because the SHCC layer was detached from the slab's edges.

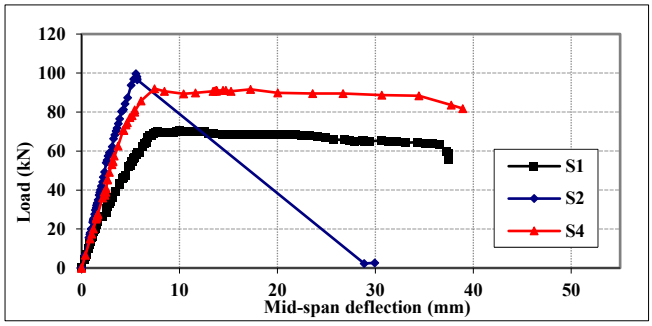

(a) Load-mid span deflection of failed span for S1, S2, and S4

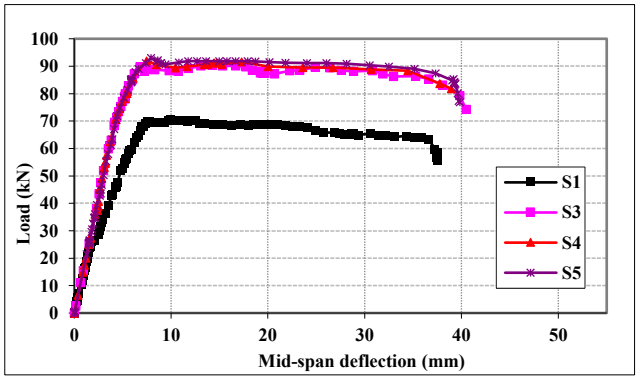

(b) Load-mid span deflection of failed span for S1, S3, S4 and S5

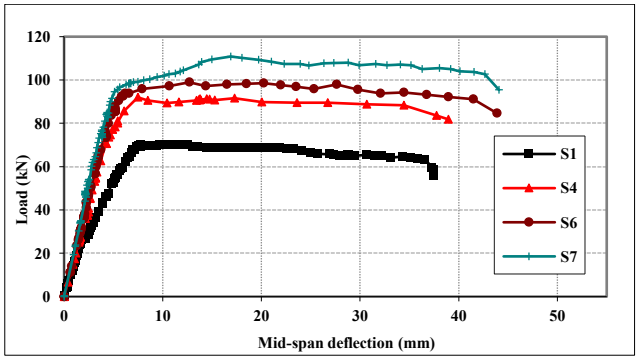

(c) Load-mid span deflection of failed span for S1, S4, S6 and S7

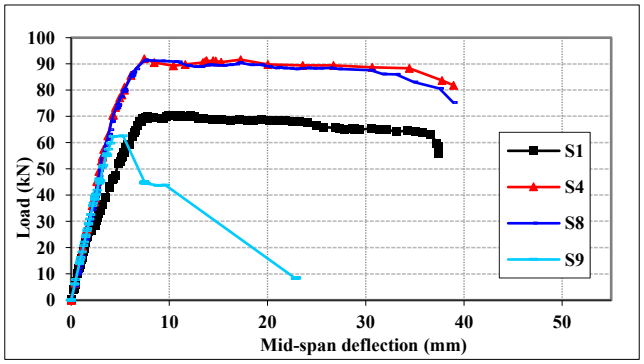

(d) Load-mid span deflection of failed span for S1, S4, S8 and S9

Fig. 10: Load-mid span deflection of failed span for all specimens

F. Ductility factor

In most cases, characteristics created as bending ductility indices were used to determine the ductility of RC members. The structural elements' ductility refers to their capacity to withstand inelastic deformation without significantly reducing their strength. The ductility is assessed using the ductility factor. The following equation was used to determine the ductility index.

$$(DF) = \Delta_u / \Delta_y \qquad (1)$$

where Δ_y represents the deflection at the steel's yield point, Δ_u represents the deflection at ultimate load, and represents the deflection ductility index.

All slabs' ductility index values were calculated based on the data in table 5 and figure 11 shows the results. The slabs S2 and S9 which failed by debonding of SHCC layer so that their results were ignored. This is due to the sudden collapse of the two slabs due to mistake in fabrication. The ductility factor slightly increased as the SHCC thickness increased on the other hand the ductility factor significantly increased by increasing the internal reinforcement ratio. The graph demonstrates that increasing the reinforcement ratios from 0.38% to 0.5% and 0.63%, respectively, increase the ductility factor by an additional 65% and 111% (reinforcement ratio increased by 31.6% and 65.8% for S_6, and S_7, respectively).

The minimum ductility index should be around 1.7 and 2.6 for concrete types C35/45 or below and concrete types greater than C35/45, respectively, according to the Fédération Internationale du Béton (FIB) standards [35]. The designation C35/45 denotes a concrete mix with a cubic compressive strength of 45 MPa and a cylinder compressive strength of 35 MPa. To avoid an abrupt failure of the reinforced flexural members, the ductility index should be greater than this minimal value. Except for slab S_1, S_2, S_3 and S_9 all of the reinforced slabs in the current study exceeded the minimal ductility index advised by FIB. According to FIB guidelines, the minimum reinforcing ratio of the SHCC layer should be 0.50% in order to meet the minimal ductility index.

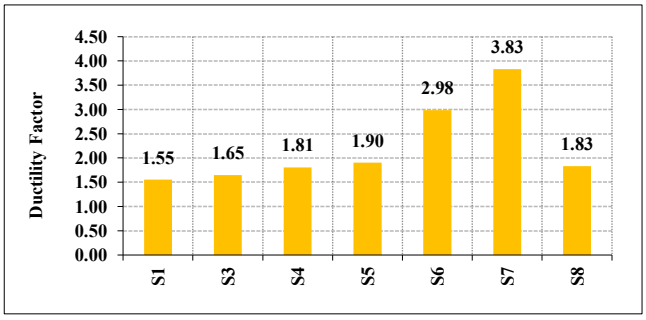

Fig. 11: Ductility factor of the test slabs

V- PREDICTION OF THE FLEXURAL CAPACITY FOR THE STRENGTHENED SLABS

The inclusion of the SHCC layer greatly improved the structural performance of the reinforced defected slabs, as shown in this work. As a result, the SHCC layer's contribution needs to be taken into account in the design calculations. For

DOI: 10.21608/ERJENG.2023.212986.1182

Journal of Engineering Research (ERJ)
Vol. 7 – No. 2, 2023
©Tanta University, Faculty of Engineering
ISSN: 2356-9441 https://erjeng.journals.ekb.eg/ e ISSN: 2735-4873

the purpose of predicting the flexural capacity, the following hypotheses were taken into account:

(1) It was anticipated that regular concrete would fail in compression.
(2) According to ACI-318 [36], the maximum concrete strain (εc_u) corresponding to the ultimate compressive stress for concrete can be considered to be 0.003.
(3) Regular concrete's tensile strength was disregarded except in unreinforced section subjected to tension S_1[37].
(4) The JSCE guidelines' presumptions were used to calculate the tensile strength given by the SHCC layer [38].
(5) The yield steel strength (f_y) was set as the maximum strength for the steel reinforcement, which was represented as elastic-plastic under stress[36].
(6) The SHCC layer is fully bonded with the RC slabs.

In the current work, the equilibrium with assumed full geometric compatibility in the member section was used to forecast the flexural capacity of the reinforced slabs. Figure 12a displays the load distribution along the slab statically system. The collapse mechanism and corresponding bending moments for test slabs may assumed as shown in figure 12b and 12c, respectively. The depiction of stresses and strains at sagging and hogging moments shown in figure 12d and 12 e, respectively

The ultimate sagging flexural capacity, M_{us}.

$$M_{us} = T_{st}[d - \alpha \cdot x/2] \quad (2)$$

$$T_{st} = A_s . f_y \quad (3)$$

Based on the equilibrium situation, it is possible to determine the depth on neutral axis (x) as follows:

$$x = T_{st}/0.85f'_c \cdot \alpha \cdot b \quad (4)$$

The ultimate hogging flexural capacity, M_{uh}.

$$M_{uh} = T_{st}\left[d - \alpha\frac{x}{2}\right] + T_{SHCC}[t - \frac{t_{SHCC}}{2} - \alpha\frac{x}{2}] \quad (5)$$

$$T_{st} = A_s . f_y \quad (6)$$

$$T_{SHCC} = f_{ty,SHCC}[A_{SHCC} - A_S] \quad (7)$$

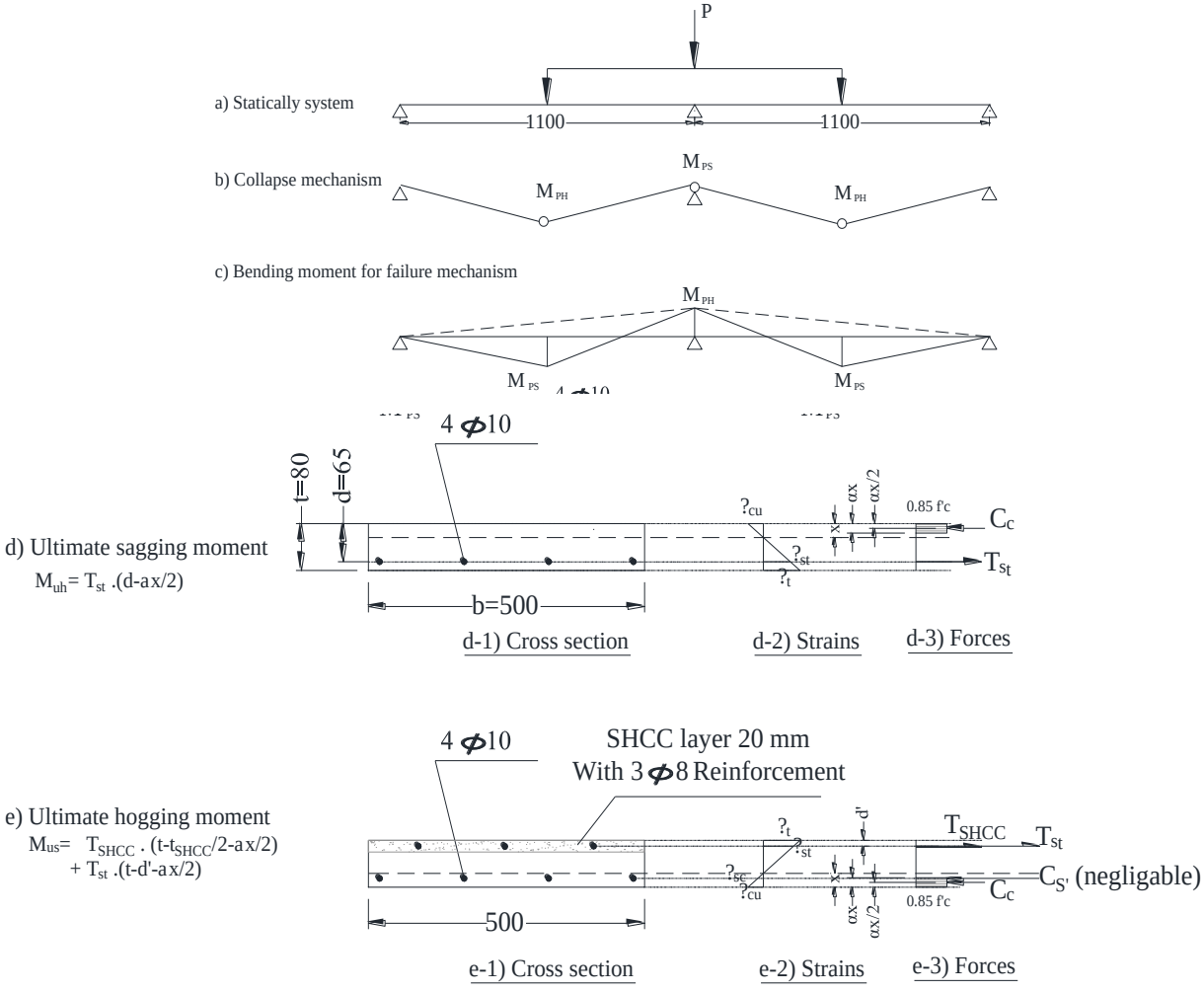

Fig. 12. Forces equilibrium at collapse mechanism for test slabs.

DOI: 10.21608/ERJENG.2023.212986.1182

Journal of Engineering Research (ERJ)
Vol. 7 – No. 2, 2023
©Tanta University, Faculty of Engineering
ISSN: 2356-9441 https://erjeng.journals.ekb.eg/ e ISSN: 2735-4873

Table 6. Test ultimate load versus predicted ultimate load.

Slab	M_{hu}	M_{su}	Predicted ultimate load P_{upr}(kN.m)	Experimental ultimate load P_{uexp} (kN.m)	P_{upr}/P_{uexp}
S_1	6.92	1.80	68.79	70	0.98
S_2	6.92	6.39	88.99	100	0.89
S_3	6.92	4.33	79.93	91	0.88
S_4	6.92	5.05	83.09	92	0.90
S_5	6.92	5.60	85.50	93	0.92
S_6	6.92	5.76	86.21	99	0.87
S_7	6.92	6.45	89.25	111	0.80

Also, based on the equilibrium situation, it is possible to determine the depth on neutral axis (x) as follows:

$$x = (T_{st} + T_{SHCC})/0.85f'_c \cdot a \cdot b \quad (8)$$

where:

C_c represent the compression forces carried by the concrete. T_{SHCC} and T_{st} are the tensile forces borne by the SHCC layer and tension steel reinforcement, respectively. f'_c and $f'_{c,SHCC}$ = the compressive strengths of concrete and SHCC, respectively. $f_{ty,\ SHCC}$ is the SHCC tensile yield strength (First cracking strength as per JSCE recommendations [38]). f_y is the yeild steel reinforcement's stress. The cross-sectional of the SHCC layer are denoted by A_{SHCC}. b is the width of the concrete section. A_s is the area of the tension steel reinforcement. d = the concrete section's effective depth. t stands for the section's overall thickness. A is the stress block factor and taken is now equal to 0.85[36]. Finally, the predicted ultimate load could be calculated from the equation:

$$Pupr = 8\,(M_{uh}/2 + M_{us})/1.1 \quad (9)$$

Table 6 lists the experimental and Predicted results. As shown in Table 6, the prediction model overestimated the control slab's flexural strength by 10-20%, leaving good safety margin for errors due to relaying on the assumptions of codes that are more cautious.

VI- CONCLUSIONS

This paper presented experimental results of nine two-span one-way slabs tested under five-point loading. The control slab was cast without top reinforcement at the internal support. The recent eight slabs were conducted to assess the impact of various parameter affected utilizing SHCC in strengthening the defected continuity on the structural response. The main parameters were the position of SHCC layer relative to the concrete section, SHCC layer thickness-to-the original slab thickness ratios (25%, 37.5%, and 50%), the imbedded reinforcement in SHCC ratios relative to the original slab thickness (0.38%, 0.5%, and 0.63%), and finally the development length-to- span length ($0.25L_n$, $0.2L_n$, and $0.15\ L_n$). The following points are the essential conclusions of this study:

1. Overlaying the SHCC layer outside the section is superior to supplanting the layer of the substantial concrete section, as the flexural stiffness and deflection resistance increases, yet consideration should be paid to the factors controlling bonding. The chance of debonding failure increases when laying the SHCC layer outside the section due to stress concentration at the areas of geometry discontinuity. The use of a SHCC layer added to the original section led to a delay in the appearance of cracks by a percentage of 20.8% and 8% in the negative and positive moments, respectively, but it was reflected in an increase in the stiffness of the slab in bending and a decrease in the ductility factor compared to removing a layer of concrete and strengthening the slab without increasing the total thickness.
2. It can likewise be inferred that by expanding the supplanting thickness of the SHCC to a thickness more than 0.25 of the slab thickness, the increment in the ultimate load and ductility is not significant. Supplanting a thickness of 0.25, 0.375, and 0.5 from existing slabs by SHCC layer with 0.38% embedded reinforcement at the negative moment regions, increases the cracking load in the hogging and sagging moment by 81-88% and 46-50% for all slabs respectively, and furthermore increases the ultimate load by 30%, 31%, and 33%, and the ductility factor by 6.45%, 16.8%, and 22.6%, respectively, compared to the control slab S_1.
3. Replacing a thickness of 0.375 from existing slabs by SHCC layer with reinforcement ratios 0.38%, 0.5%, and 0.63% (ratios relative to the original slab thickness) embedded at the negative moment regions increases the cracking load in the positive region by 50%, 57.7%, and 69.5%, the cracking load in the negative region by 88.4%, 100%, and 111.5%, the ultimate load by 31.4% and 41.43%, and 58.6%, and the ductility by 16.8%, 86%, and 147%, respectively, compared to the control slab.
4. It isn't prescribed to lessen the development length of the SHCC layer to 0.15 of the clear spans in case of one-way slabs supported line loads, on the grounds that the slab failed outside the strengthening layer due to the short advancement length. It is prescribed to utilize the SHCC layer with a development length of at least 0.2 of the clear spans since it is prudent and gives results indistinguishable from the slab with a development length of 0.25 length of the clear span.
5. The flexural capacity of the test slabs is generally underestimated by the suggested flexural prediction model based on forces equilibrium. The analytical/experimental results' average value ranged from 0.8 to 0.9, providing a good margin of error.

Funding: This research has not received any type of funding.

Conflicts of Interest: The authors declare there is no conflict of interest.

DOI: 10.21608/ERJENG.2023.212986.1182

Journal of Engineering Research (ERJ)
Vol. 7 – No. 2, 2023
©Tanta University, Faculty of Engineering
ISSN: 2356-9441 https://erjeng.journals.ekb.eg/ e ISSN: 2735-4873

REFERENCES

[1] 1. Fayed, S. Flexural Strengthening of Defected RC Slabs Using Strain-Hardening Cementitious Composites (SHCC): An Experimental Work. Arab. J. Sci. Eng. 2020, 45, 3731–3742, doi:10.1007/s13369-019-04219-5.

[2] 2. Yu, K.; Li, L.; Yu, J.; Wang, Y.; Ye, J.; Xu, Q.F. 1Direct tensile properties of engineered cementitious composites: A review. Constr. Build. Mater. 2018, 165, 346–362, doi:10.1016/j.conbuildmat.2017.12.124.

[3] 3. Bonaldo, E.; de Barros, J.A.; Lourenço, P.B. Efficient Strengthening Technique to Increase the Flexural Resistance of Existing RC Slabs. J. Compos. Constr. 2008, 12, 149–159, doi:10.1061/(asce)1090-0268(2008)12:2(149).

[4] 4. Bolander, J.E.; Berton, S. Simulation of shrinkage induced cracking in cement composite overlays. Cem. Concr. Compos. 2004, 26, 861–871, doi:10.1016/j.cemconcomp.2003.04.001.

[5] 5. Barros, J.A.O.; Cunha, V.M.C.F.; Ribeiro, A.F.; Antunes, J.A.B. Post-cracking behaviour of steel fibre reinforced concrete. Mater. Struct. Constr. 2005, 38, 47–56, doi:10.1617/14058.

[6] 6. Almassri, B.; Halahla, A.M. Corroded RC beam repaired in flexure using NSM CFRP rod and an external steel plate. Structures 2020, 27, 343–351, doi:10.1016/j.istruc.2020.05.054.

[7] 7. Arslan, G.; Sevuk, F.; Ekiz, I. Steel plate contribution to load-carrying capacity of retrofitted RC beams. Constr. Build. Mater. 2008, 22, 143–153, doi:10.1016/j.conbuildmat.2006.10.009.

[8] 8. Su, R.K.L.; Zhu, Y. Experimental and numerical studies of external steel plate strengthened reinforced concrete coupling beams. Eng. Struct. 2005, 27, 1537–1550, doi:10.1016/j.engstruct.2005.04.012.

[9] 9. Vasquez, A.; Karbhari, V.M. Fiber-Reinforced Polymer Composite Strengthening of Concrete Slabs with Cutouts. ACI Struct. J. 2003, 100, 665–673, doi:10.14359/12808.

[10] 10. Tan, K.H.; Zhao, H. Strengthening of Openings in One-Way Reinforced-Concrete Slabs Using Carbon Fiber-Reinforced Polymer Systems. J. Compos. Constr. 2004, 8, 393–402, doi:10.1061/(asce)1090-0268(2004)8:5(393).

[11] 11. Teng, J.G.; Smith, S.T.; Yao, J.; Chen, J.F. Intermediate crack-induced debonding in RC beams and slabs. Constr. Build. Mater. 2003, 17, 447–462, doi:10.1016/S0950-0618(03)00043-6.

[12] 12. El-Hacha, R.; Rizkalla, S.H. Near-surface-mounted fiber-reinforced polymer reinforcements for flexural strengthening of concrete structures. ACI Struct. J. 2004, 101, 717–726.

[13] 13. De Lorenzis, L.; Teng, J.G. Near-surface mounted FRP reinforcement: An emerging technique for strengthening structures. Compos. Part B Eng. 2007, 38, 119–143, doi:10.1016/j.compositesb.2006.08.003.

[14] 14. J.1151-2916.1995.Tb07979.X.Pdf.

[15] 15. Li, L.Z.; Bai, Y.; Yu, K.Q.; Yu, J.T.; Lu, Z.D. Reinforced high-strength engineered cementitious composite (ECC) columns under eccentric compression: Experiment and theoretical model. Eng. Struct. 2019, 198, 109541, doi:10.1016/j.engstruct.2019.109541.

[16] 16. Li, L.; Cai, Z.; Yu, K.; Zhang, Y.X.; Ding, Y. Performance-based design of all-grade strain hardening cementitious composites with compressive strengths from 40 MPa to 120 MPa. Cem. Concr. Compos. 2019, 97, 202–217, doi:10.1016/j.cemconcomp.2019.01.001.

[17] 17. Lim, Y.M.; Li, V.C. Durable repair of aged infrastructures using trapping mechanism of engineered cementitious composites. Cem. Concr. Compos. 1997, 19, 373–385, doi:10.1016/S0958-9465(97)00026-7.

[18] 18. SUTHIWARAPIRAK, P.; MATSUMOTO, T.; KANDA, T. Flexural Fatigue Failure Characteristics of an Engineered Cementitious Composite and Polymer Cement Mortars. Doboku Gakkai Ronbunshu 2002, 2002, 121–134, doi:10.2208/jscej.2002.718_121.

[19] 19. Till, R. Final Report on Durable Link Slabs for Jointless Bridge Decks Based on Strain-Hardening Cementitious Composites By M . Lepech , S . Qian , M . Weimann and S . Wang The Advanced Civil Engineering Material Research Laboratory Department of Civil and Environ. 2003.

[20] 20. Mündecke, E.; Mechtcherine, V. Tensile behaviour of strain-hardening cement-based composites (SHCC) with steel reinforcing bars. Cem. Concr. Compos. 2020, 105, 103423, doi:10.1016/j.cemconcomp.2019.103423.

[21] 21. Li, J.; Weng, J.; Yang, E.H. Stochastic model of tensile behavior of strain-hardening cementitious composites (SHCCs). Cem. Concr. Res. 2019, 124, 105856, doi:10.1016/j.cemconres.2019.105856.

[22] 22. Fischer, G.; Li, V.C. Influence of matrix ductility on tension-stiffening behavior of steel reinforced engineered cementitious composites (ECC). ACI Struct. J. 2002, 99, 104–111, doi:10.14359/11041.

[23] 23. Kunieda, M.; Hussein, M.; Ueda, N.; Nakamura, H. Enhancement of crack distribution of UHP-SHCC under axial tension using steel reinforcement. J. Adv. Concr. Technol. 2010, 8, 49–57, doi:10.3151/jact.8.49.

[24] 24. Bridges, M.S.; City, Q. Medium Span Bridges Exprimental Investigation On Externally Prestressed Segmental Bridges Under Torsion Using Different JOINTS. 2018, 1–11.

[25] 25. Afefy, H.M.; Abdel-Aziz, M.A.; Kassem, N.M.; Mahmoud, M.H. Improving flexural performance of post-tensioned pre-cast pre-stressed RC segmental T-beams. Structures 2020, 24, 304–316, doi:10.1016/j.istruc.2020.01.027.

[26] 26. Khalil, A.E.A.; Atta, A.M.; Hassan, A.; Abd-Elaaty, A.H. Flexural strength recovery of RC one-way slabs having cut-outs using NSM-SHCC plates. Eng. Struct. 2022, 258, 114149, doi:10.1016/j.engstruct.2022.114149.

[27] 27. Abbas, Y.M.; Iqbal Khan, M. Fiber–Matrix Interactions in Fiber-Reinforced Concrete: A Review. Arab. J. Sci. Eng. 2016, 41, 1183–1198, doi:10.1007/s13369-016-2099-1.

[28] 28. Chung, K.L.; Ghannam, M.; Zhang, C. Effect of Specimen Shapes on Compressive Strength of Engineered Cementitious Composites (ECCs) with Different Values of Water-to-Binder Ratio and PVA Fiber. Arab. J. Sci. Eng. 2018, 43, 1825–1837, doi:10.1007/s13369-017-2776-8.

[29] 29. Maalej, M.; Lin, V.W.J.; Nguyen, M.P.; Quek, S.T. Engineered cementitious composites for effective strengthening of unreinforced masonry walls. Eng. Struct. 2010, 32, 2432–2439, doi:10.1016/j.engstruct.2010.04.017.

[30] 30. Dehghani, A.; Nateghi-Alahi, F.; Fischer, G. Engineered cementitious composites for strengthening masonry infilled reinforced concrete frames. Eng. Struct. 2015, 105, 197–208, doi:10.1016/j.engstruct.2015.10.013.

[31] 31. Kesner, K.; Billington, S.L. Investigation of Infill Panels Made from Engineered Cementitious Composites for Seismic Strengthening and Retrofit. J. Struct. Eng. 2005, 131, 1712–1720, doi:10.1061/(asce)0733-9445(2005)131:11(1712).

[32] 32. Maalej, M.; Leong, K.S. Engineered cementitious composites for effective FRP-strengthening of RC beams. Compos. Sci. Technol. 2005, 65, 1120–1128, doi:10.1016/j.compscitech.2004.11.007.

[33] 33. Dai, J.G.; Wang, B.; Xu, S.L. Textile reinforced engineered cementitious composites (TR-ECC) overlays for the strengthening of RC beams. APFIS 2009 - Asia-Pacific Conf. FRP Struct. 2009, 75–80.

[34] 34. Egyptian code for design and construction of reinforced concrete structures (ECP 203-2020); 2020.

[35] 35. Fédération Internationale du Béton (FIB) Externally bonded FRP reinforcement for RC structures. Bulletin 14, Lausanne, Switzerland, pp. 138, 2001.

[36] 36. ACI Committee 318 (2019). Building Code Requirements for Structural Concrete (ACI 318-19) and Commentary (ACI 318R-19). American Concrete Institute, Farmington Hills, MI, 519 pp.

[37] 37. Yang EH, Yang Y, Li VC. Use of high volumes of fly ash to improve ECC mechanical properties and material greenness. ACI Mater J 2007;104(6):303–11.

[38] 38. Japan Society of Civil Engineers (JSCE). Recommendations for design and construction of high performance fiber reinforced cement composite with multiple fine cracks (HPFRCC), Concrete engineering series 82; 2008.